Journal of Applied Polymer Science

Synthesis and characterization of partially hydrolyzed polyacrylamide nanocomposite weak gels with high molecular weights

Jingshui Xu,[1] Denglong Chen,[1] Yangchuan Ke,[2] Li Yang,[2] Xin Bai,[1] Guoliang Zhang,[2] Zheling Zeng,[3] Wenshuai Gao,[3] Deming Gong[4]

[1]Quangang Research Institute of Petrochemical Technology, Fujian Normal University, Fuzhou 362807, China
[2]State Key Laboratory of Heavy Oil Processing, College of Science, China University of Petroleum, Beijing 102249, China
[3]School of Environmental and Chemical Engineering, Nanchang University, Nanchang 330047, China
[4]School of Biological Sciences, University of Auckland, Private Bag 92019, Auckland, New Zealand
Correspondence to: Y. Ke (E-mail: kyc001@sohu.com)

ABSTRACT: High-molecular-weight partially hydrolyzed polyacrylamide nanocomposite (HPAMNC) weak gels were synthesized and evaluated for their flooding behaviors in oil-recovery applications. The structure, morphology, and properties of the obtained HPAMNC samples and their weak gels were characterized by X-ray diffraction (XRD), transmission electron microscopy (TEM), and scanning electron microscopy (SEM). XRD patterns clearly proved the exfoliation of the montmorillonite (MMT) layers in the polymer matrix; this was consistent with TEM analysis. The morphology of the HPAMNC was proven to be in a cross-wire aggregated form by SEM analysis. The viscosity-average molecular mass of the obtained HPAMNC was approximately 8.51×10^6 under the optimized MMT load at 1.0 wt %. The flooding experiments showed that the oil-recovery rates in sand pack tubes with low and high permeability were enhanced by approximately 35.1 and 46.2%, respectively. © 2015 Wiley Periodicals, Inc. J. Appl. Polym. Sci. **2015**, *132*, 42626.

KEYWORDS: clay; crosslinking; gels; nanostructured polymers

Received 9 December 2014; accepted 14 June 2015
DOI: 10.1002/app.42626

INTRODUCTION

Polymeric hydrogels produced by the reaction between a polymer and crosslinker consist of a three-dimensional polymer network and the water-bounding interstitial space of the network.[1,2] These hydrogels are being used in an increasing number of applications, such as carriers for proteins and nucleic acids in gel electrophoresis and for the control of excess water production in chemically enhanced oil recovery through profile modification or blocking the path with highly permeable water.[3,4] In these applications, information on the molecular constitution of the hydrogels and their elastic properties is critical.[5] Polymeric hydrogels are usually produced by the free-radical copolymerization of acrylamide (AM)-based monomers with a chemical crosslinker, such as *N*,*N*′-methylene bisacrylamide, in an aqueous solution.[1] However, these polymeric hydrogels are usually soft and fragile when they are handled in the swollen state because of the presence of water in the gel-formation process.[6,7] To produce high-quality polymeric hydrogels, many new techniques have been applied to improve their mechanical properties.

Recently, nanocomposite gels have been developed that can overcome the limitations of the mechanical properties of conventional polymeric hydrogels.[8,9] Nanocomposite gels have been designed by *in situ* polymerized silica or titania nanoparticles together with organic crosslinkers.[10,11] Such effects have been not obvious in improving the mechanical properties through the incorporation of these inorganic nanoparticles. This is because they do not act as effective reinforcing agents in toughening these nanocomposite gels.[12] However, polyacrylamide (PAM)/montmorillonite (MMT) nanocomposite gels obtained with exfoliated MMT layers instead of organic crosslinkers can dramatically improve their mechanical properties, including their stiffness, thermal stability, and strength.[13,14] This is mainly because of the unique organic/inorganic network structures in these PAM/MMT nanocomposite gels. In this structure, the MMT layers are not only the reinforcement but also an important constituent in improving the physical properties of the nanocomposite gels.[15–17] Thus, it could be inferred that nanocomposite gels crosslinked with exfoliated inorganic MMT layers have extraordinarily high mechanical properties. A practical application of these PAM/MMT nanocomposite gels is in circulation channels in oilfield development, where water is injected into the oil formation to enhance oil yield. Because water prefers to flow along the more highly permeable channels

and because of the preponderance of the flow path, this leads to excessive water waste and rapid decline in productivity.[18] Because of this reason, many chemical reagents have been designed and tested in heterogeneous oil formation to improve the water-injection profiles in water-injection wells.[19] Chemical gels of diverse sizes of high-temperature tolerance and *in situ* gels have been tried for many years.[20] Among these gels, the partially hydrolyzed PAM-based crosslinked gels are the most widely used gel systems; they are designed to decrease the water permeability or degree of water coning; this results in an increase in the oil sweep efficiency in enhanced oil-recovery stages.[21,22] Similar to the crosslinked polymer solution, under the optimized conditions of chain coil size and size distribution, these gels form effective flooding in the pore or fracture channels in the rock cores and homogenize the core permeability.[23] These gels, as they go through the core channels, are tunable with ball-like or cross-wire morphologies, where they wriggle themselves inside the multisize formation channels to exert a sweep effect on the residual oil.[24] However, these gels are unstable or degradable under application conditions such as high temperature (>80°C), high pH value, saline conditions, and mechanical shearing.[25,26] To overcome the previous complicated conditions in oil reservoirs, the redesign of nanocomposite gels with stronger mechanical properties is needed. In a previous study, we reported that well-tunable MMT layer dispersion in the polymer matrix could effectively improve the physicochemical properties, such as thermal stability, swelling, wettability, and mechanical properties.[27] However, in PAM/MMT nanocomposites, the good tuning of the MMT layer dispersions in the PAM matrix, which has direct effects on the polymer morphology and application properties, is still a big challenge in petroleum engineering.[21,22,28,29]

In this study, novel, partially hydrolyzed polyacrylamide nanocomposites (HPAMNCs) with a high molecular weight [viscosity-average molecular mass (M_η)] and their weak gels were successfully synthesized from AM monomers, montmorillonite intermediates (I-MMTs), and chromium [Cr(III)], in which MMT layers with a high aspect ratio were exfoliated through the polymer matrix and acted as multifunctional crosslinkers. The morphologies and structures of the MMT platelet dispersion in the polymer matrix were examined by scanning electron microscopy (SEM), X-ray diffraction (XRD), and transmission electron microscopy (TEM). The salt tolerance, temperature tolerance, and shear tolerance were measured, and the flooding behavior of the nanocomposite weak gels was investigated in sand pack tube models.

EXPERIMENTAL

Materials

Unmodified sodium montmorillonite (Na-MMT; moisture content < 10%, [SiO_2] = 48.0–51.0%, [Al_2O_3] = 13.0–16.0%, [MgO] = 3.721%, [CaO] = 3.712%, Fe_2O_3 = 1.858%, K_2O = 0.748%), with a cationic-exchange capacity of 100 mmol/100 g, was obtained from Huai An Saibei Technology Co., Ltd. (China). AM (>98.0% purity) was purchased from Jiangxi Chang Jiu Agrochemical Co., Ltd. (China). Ethylenediamine tetraacetic acid disodium salt [EDTA–2Na; analytical reagent (AR)] and hexadecyl trimethyl ammonium chloride (AR) were purchased from Tianjing Guangfu Fine Chemical Limited Co., Ltd. (China). Ethanolamine (AR) and phosphoric acid (AR, 98%) were purchased from Tianjing Guangfu Fine Chemical Research Institute (China). Ammonium peroxydisulfate [$(NH_4)_2S_2O_8$; AR] and sodium bisulfite ($NaHSO_3$; AR) were purchased from Beijing Modern Eastern Chemical Reagent Co., Ltd. (China). Urea [$CO(NH_2)_2$; AR], sodium hydroxide (AR), and sodium chloride (NaCl; AR) were purchased from Beijing Modern Eastern Chemical Reagent Co., Ltd. (China). A chromium compound (SC-1 type) with a main component of [$(Cr(H_2O)_6)^{3+}$; AR] was produced at the Oil Recovery Institute, Sheng Li Oilfield (China). Other reagents (AR) were purchased from Xilong Chemical Co., Ltd. (China).

Preparation of Weak Gels of PAM Nanocomposites with MMT

Preparation of I-MMT. Na-MMT (30.0 g) was immersed in 600 mL of deionized water for 30 min in a 1000-mL, three-necked flask with a stirrer and a thermometer. Hexadecyl trimethyl ammonium chloride (3.68 g), ethanolamine (1.4 g), and phosphoric acid (2.0 mL) were dissolved in 25 mL of deionized water in a 100-mL beaker and then added dropwise to the Na-MMT dispersion at 80°C with continuous stirring. The cationic exchange was carried out at 80°C for 16 h under the ventilation of nitrogen gas to form a viscous mixture (mixture A). Then, AM (95 wt % Na-MMT) was added to mixture A in a flask at 65°C under a nitrogen gas atmosphere to form mixture B after reaction for an additional 4 h. Then, mixture B was cooled down to 30°C; at that point, 0.08 wt % $(NH_4)_2S_2O_8$ was added and reacted for another 4 h. The total reaction lasted for 32 h, and inorganic I-MMT was obtained.

Synthesis of HPAMNC. An amount of 25.0 g of AM was diluted into 100 g of deionized water in a 500-mL, three-necked flask with a stirrer and a thermometer and cooled in an ice water bath. $CO(NH_2)_2$ (0.02–0.10 wt %) and EDTA–2Na (0.02–0.10 wt %) were added to the AM solution; then, NaOH (5.0% w/w) was added dropwise to the three-necked flask to adjust the pH to 10.5. The obtained I-MMT suspension was slowly added to the three-necked flask at a constant stirring rate (300 rpm) to form a good suspension. Then, the reaction solution was poured into an adiabatic reaction with a thermometer. Nitrogen gas flowed into the reaction to remove oxygen for 20 min. Then, $(NH_4)_2S_2O_8$ (0.02–0.08 wt %) and $NaHSO_3$ (0.02–0.08 wt %) were added to the reaction solution to polymerize for 3 h. Thus, the PAM nanocomposites were prepared.

To obtain the high-M_η HPAMNCs, the hydrolysis reaction for the preparation of PAM nanocomposite was performed according to a previous report by Rabiee *et al.*[30] with a slight modification. The obtained PAM nanocomposites were hydrolyzed by solid sodium hydroxide (0.2–8.0 wt %) at 100°C in a sealed oven for 4 h. Then, the samples were dried at 60°C for 24 h. Finally, the HPAMNC samples were crushed and collected for further analysis.

Synthesis of the HPAMNC Weak Gels. The HPAMNC weak gels were prepared according to a previous report by Jamal and Ali[31] with a slight modification. An amount of 6.0 g of the obtained HPAMNC powder ($M_\eta \approx 8.15 \times 10^6$) was completely

dissolved in a 2.0-L NaCl solution (5.0 g/L) in a 5.0-L beaker with continuous stirring to form the mother solution, which was placed at 28°C for 24 h. A crosslinker mixture system (2.0–5.0 wt % of the obtained HPAMNC), which consisted of the chromium aqueous solution (1.0 g/L) and the stabilizer of thiourea (0.2 g/L), was diluted with NaCl solution (5.0 g/L). Then, the crosslinker mixture was added to the mother solution with continuous stirring and sealed in a steel autoclave at 80°C for about 2 days. Finally, the HPAMNC weak gel solution was formed and collected.

Characterization

XRD analysis was performed on Bruker D8 Advance X-ray diffractometer (STADI P, Germany) with a Cu target ($\lambda = 0.1540$ nm) at room temperature. The system consisted of a rotating anode generator operated at 40 kV and with a 40-mA current. The scanned diffraction angle (2θ) was scanned from 1.3 to 10° at a scanning rate of 1°/min and a step distance of 0.02°. Bragg's law was applied to calculate the distance between the silicate layers:[26]

$$2d \sin\ \theta = n\lambda \quad (1)$$

Where, $n = 1$, λ is the wavelength of the X-ray, d is the diffraction interplanar distance (nm), and 2θ is diffraction angle (°).

The particle size and size distribution in the HPAMNC weak gel were measured with a trial-and-error process in a diluted solution by dynamic laser light scattering (Malvern laser nanoparticle size analyzer, Malvern Co.). The apparent viscosities of samples were measured by a MCR101 rheometer (Anto Paar Gmbh, Austria).

The intrinsic viscosities ([η]s) and relative M_η values of the samples were measured by an automatic Ubbelohde capillary viscometer at 25 ± 0.1°C. The diameter of the capillary tube was 0.56 mm, and the average shear rate in the tube was about 1500 s^{-1}. All of the solutions were prepared in the same way as described in the literature.[32] The solvents were filtered through 0.1-μm Millipore filters. The M_η values of the samples were calculated from the Mark–Houwink equation:[33]

$$\eta_r = t/t_0 \quad (2)$$

$$[\eta] = [2(\eta_r - 1 - \ln\ \eta_r)]^{1/2}/m \cdot s \quad (3)$$

$$M_\eta = 1.563 \times [\eta]^{1.515} \times 10^5 \quad (4)$$

where η_r is the relative viscosity, t is the time that the sample solution needs to flow through the Ubbelohde viscometer; t_0 is the time that the NaCl solution (1.0 mol/L) needs to flow through the Ubbelohde capillary viscometer, m is the sample mass, and s is the solid content.

SEM (FEI Quanta 200F) was used to determine the surface morphologies of the dried gel beads. These dried gel beads were coated with a thin layer of gold to prevent charging before the SEM examinations. SEM micrographs were taken at an operating voltage of 15 kV.

The nanoparticle dispersion within the polymer matrix and the nanocomposite structure was determined with TEM (JEM-2100, Japan) at an accelerating voltage of 200 kV. The samples for TEM were ground into powder and evenly dispersed in ethanol solution. Then, the solution droplets were adsorbed in a drop-

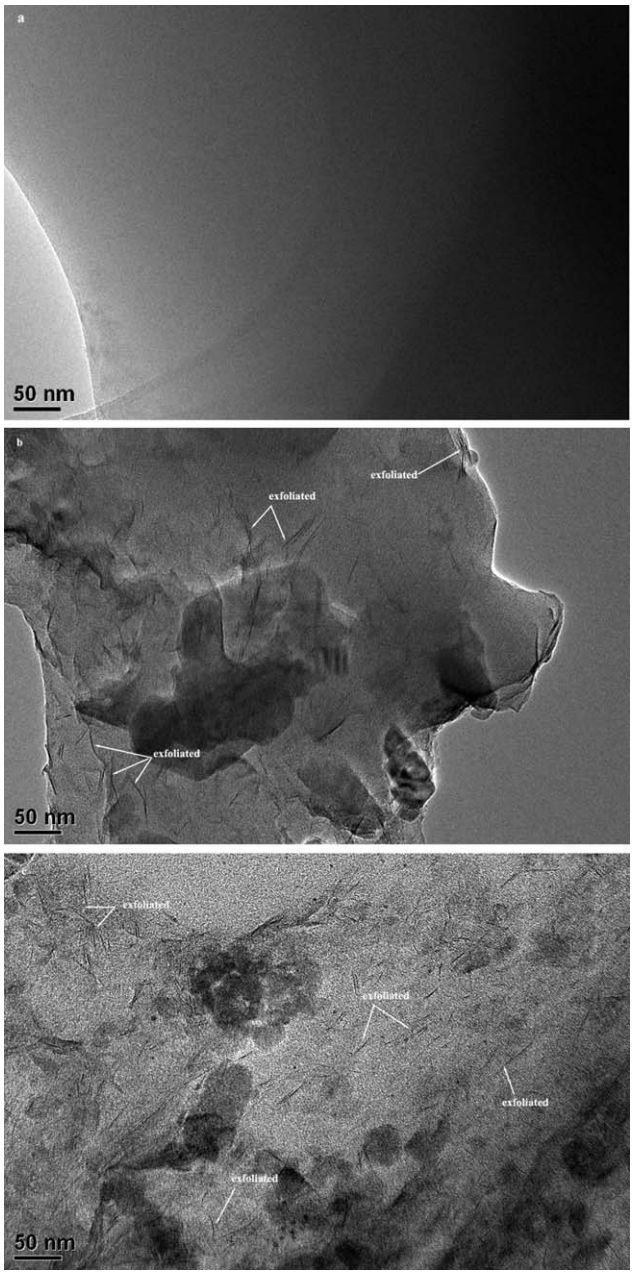

Figure 1. TEM micrographs of the (a) pure PAM, (b) HPAMNC/1.0 wt % I-MMT nanocomposite sample, and (c) HPAMNC/2.0 wt % I-MMT nanocomposite sample.

per and added to copper. This process was repeated several times. The copper with samples was dried under a UV lamp. Because MMT had a much higher electron density than the copolymer matrix, its morphology appeared as dark lines in the TEM micrographs (as shown Figure 1).

Thermal Analysis

Air atmosphere thermogravimetric refers to the imitation of the weightlessness of materials in air. This experiment was performed in an oven to investigate the thermal stability at a fixed temperature under air (e.g., 90, 120, and 150°C). Briefly, 0.5–1.0 g of sample powder was put in the oven, taken out

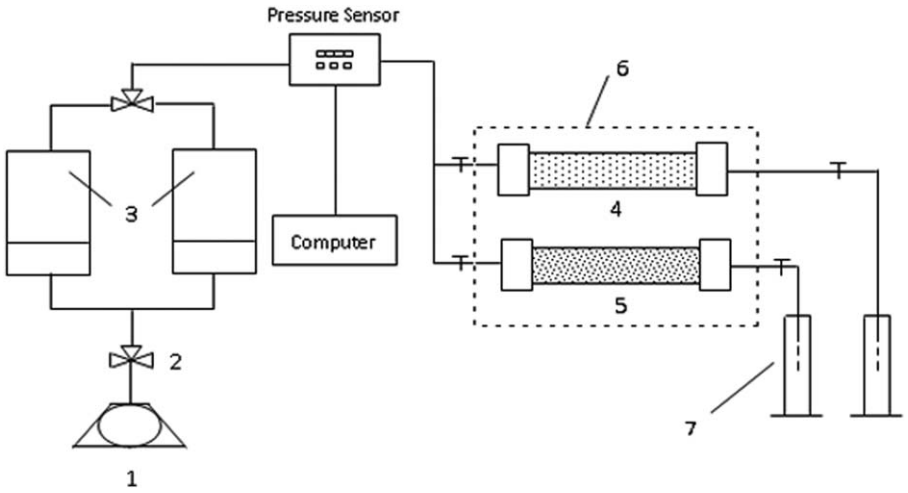

Figure 2. Flooding experimental device for weak gel suspensions: (1) constant flow pump, (2) three-way valve, (3) weak gel suspension container, (4,5) sand pack tube, (6) constant temperature sand bath, and (7) receiving container.

every 30 min, and immediately put in a desiccator until it cooled. Then, the whole sample was weighed. This test was repeated five times for each specimen to confirm its repeatability. The mass loss (M_L) was calculated with the following equation:

$$M_L = \frac{m_0 - m_t}{m_0} \times 100 \quad (5)$$

where m_0 and m_t are the weights of the original (before the oven) and degraded (after the oven) specimens, respectively.

Fluid Flow and Flooding Behaviors of the HPAMNC Weak Gel Suspensions

Experimental Conditions. The obtained HPAMNC samples with 1.0 wt % I-MMT ($M_\eta \approx 8.5 \times 10^6$) were used to prepare a solution with a concentration of 4000 mg/L. The concentration of the chromium crosslinker was 1200 mg/L. The concentration of the NaCl solution was 5000 mg/L. The simulation oil was a mixture of crude oil (Gudao region, Shengli Oilfield, China), and kerosene with a viscosity of about 80 mPa s at 70°C. The flooding behavior of the samples was measured in the sand pack tube model whose inner diameter and length were 3.8 cm and 100 cm, respectively. These sand pack tube models were all made by sand from Gudao Oilfield (China), and the sand was treated by screening, washing, and drying before use.

Flooding Experimental Procedure. The sand pack tube with low permeability was filled with a certain percentage of quartz sand with a specific surface area of 200–250 mesh (75–58 μm). The highly permeable sand pack tube was filled with quartz sand with a specific surface area of 160–180 mesh (96–86 μm). Then, the two sand pack tubes were submerged and saturated in a synthetic brine solution to measure their permeability and porosity. The saturated simulation oil was introduced into the two tubes from the inlet. The two sand pack tubes were connected, and equipped together in a fluid-flooding device (see Figure 2).

The water-flooding process was begun with a fluid flow of 1.0 mL/min until the fluids in the tube outlet contained more than 95% water. In this process, both oil and water flowed out from the sand pack tubes, and then, the fluid recovery was calculated.

The flooding process was as follows. First, 0.3 porous volume of the weak gel solution was injected at a flow rate of 1.0 mL/min into the sand pack tube model. Second, all valves were closed and left at 70°C for gel formation for approximately 30 min. Finally, the saline was injected into the same sand pack tubes at 1.0 mL/min until the fluids in the tube outlet contained more than 95% water again. Then, the oil-recovery rate was calculated according to both the oil and water volumes.

RESULTS AND DISCUSSION

Design of I-MMT and Preparation Process of the HPAMNC Samples

Design of the I-MMT Structure. Na-MMT is one of the most widely used layered silicates in PAM–clay nanocomposite gels because its lamellar elements display a high in-plane strength, stiffness, and a high aspect ratio.[13] However, pristine Na-MMT has incompatibility and a low interlayer distance; this results in a poor compatibility with the polymer matrix. For these reasons, an I-MMT was designed. In this study, as the layer-structured MMT was modified with intercalant molecules, the MMT interlayer distance (d_1) was enlarged to d_2 (namely, $d_2 > d_1$). After that, as the monomer molecule was further intercalated inside I-MMT, its interlayer distance (d_3) became larger and larger. That is, $d_3 > d_2 > d_1$. So, the inorganic I-MMT was obtained.

I-MMT Dispersion in the Polymer Matrix. The procedure for I-MMT dispersion in the PAM matrix is shown in Figure 3. Initially, the surface hydrophobicity of I-MMT was obtained by an ion-exchange process between Na-MMT and intercalants or surfactant salts. Second, the reaction system was formed through the dispersion of I-MMT in an aqueous solution of monomers at room temperature. Finally, the polymerization reactor was fixed with an adiabatic reaction with a thermometer. In the early stage

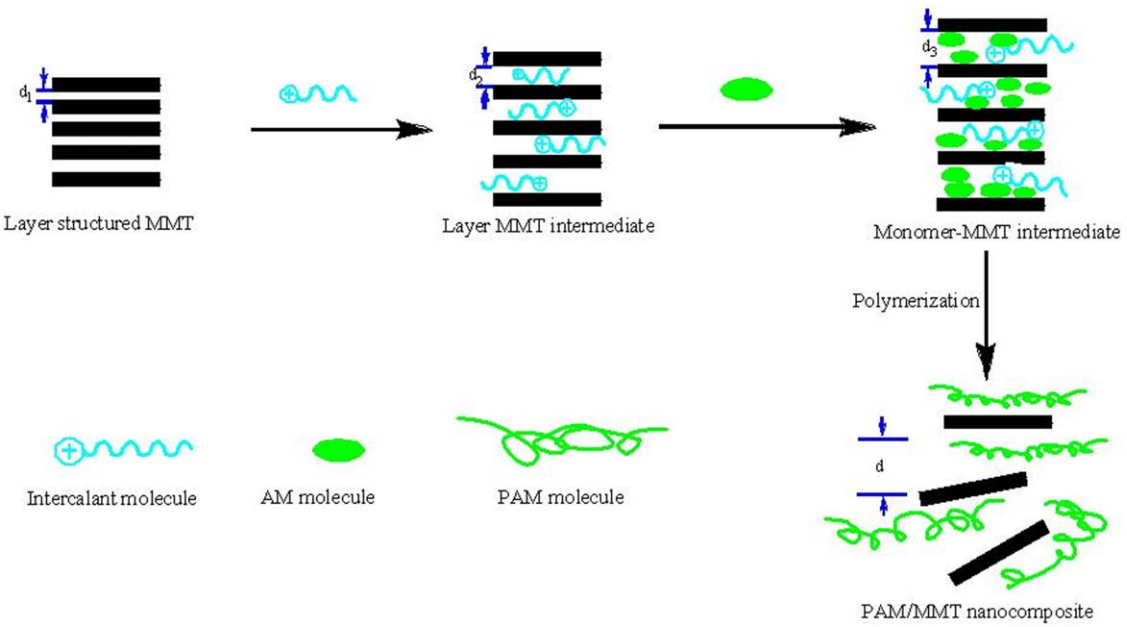

Figure 3. Diagrams showing the I-MMT structure and its tunable dispersion process in the formation of HPAMNC samples (d_1 is the spacing of Na-MMT, d_2 is the spacing of layer I-MMT, d_3 is the spacing of monomer–I-MMT, and d is the spacing of the PAN/MMT nanocomposite). [Color figure can be viewed in the online issue, which is available at wileyonlinelibrary.com.]

of polymerization, the oligomers were produced and adsorbed onto the I-MMT particles' surface by hydrogen bonding or dipole–dipole interactions;[27] these became the loci of further polymerization. Such an I-MMT structure may have been effective for creating mobility in the inorganic phase inside the PAM matrix. As for the AM monomers, the migration of I-MMT particles toward the latex particle surface became difficult as the monomer conversion increased. Thus, the step-by-step polymerization of the AM monomers was used to tune the oligomer viscosity and make the MMT platelets disperse *in situ* inside the viscose PAM matrix. These processes might have led to an exfoliated structure or intercalated structures in HPAMNC. These results were verified by XRD and TEM (see Figures 4 and 5).

XRD Analysis

An XRD technique was used to determine whether the samples had an exfoliated or intercalated structure. The XRD patterns of the pristine Na-MMT, I-MMT, and HPAMNC with (1.0 and 2.0 wt %) I-MMT load are shown in Figure 6. The diffraction peaks of the Na-MMT and I-MMT samples were found to appear at 2θ values of 7.48 and 6.21°, respectively. The interlayer distances of the Na-MMT and I-MMT samples from the Bragg's equation were 1.18 and 1.42 nm, respectively [Figure

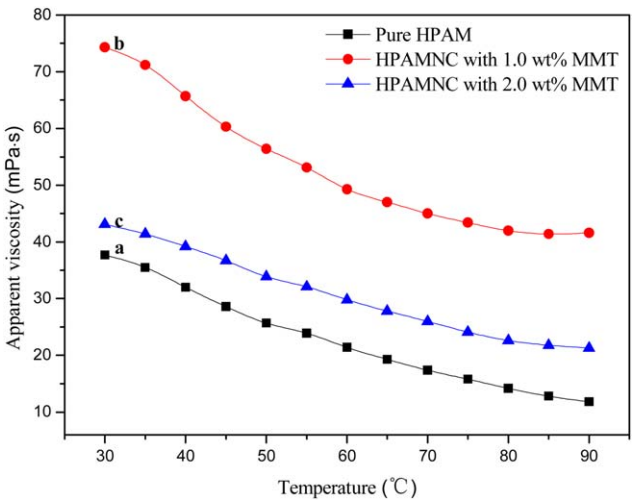

Figure 4. Curves of the apparent viscosity versus the temperature for samples of (a) pure PAM, (b) HPAMNC with 1.0 wt % I-MMT, and (c) HPAMNC with 2.0 wt % I-MMT. [Color figure can be viewed in the online issue, which is available at wileyonlinelibrary.com.]

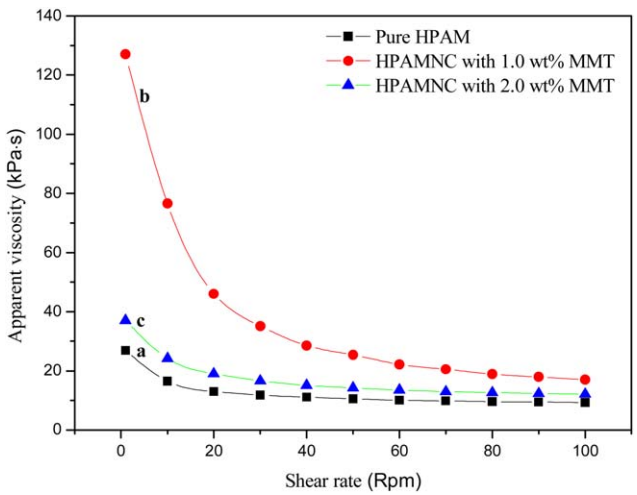

Figure 5. Curves of the apparent viscosity versus the shear rate for samples of the (a) pure PAM, (b) HPAMNC with 1.0 wt % I-MMT, and (c) HPAMNC with 2.0 wt % I-MMT. [Color figure can be viewed in the online issue, which is available at wileyonlinelibrary.com.]

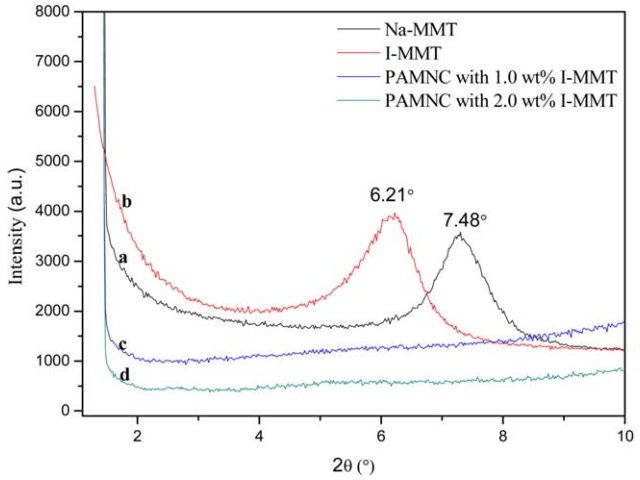

Figure 6. XRD patterns of (a) Na-MMT, (b) I-MMT, (c) HPAMNC with 1.0 wt % I-MMT, and (d) HPAMNC with 2.0 wt % I-MMT. [Color figure can be viewed in the online issue, which is available at wileyonlinelibrary.com.]

6(a,b)]. In Figure 6(c,d), no distinct peaks were observed in the XRD patterns of the nanocomposite samples. The strong peak at a 2θ of 6.21° for the typical interlayer spacing of I-MMT disappeared in these nanocomposite samples with I-MMT loads of 1.0–2.0 wt %. These results indicate that the MMT tactoids were found to be exfoliated and dispersed inside the polymer matrix at the molecular level.[33] However, X-ray scattering patterns are more feasible methods for distinguishing intercalated MMT platelets from exfoliated structures of polymer matrices. Through direct TEM observation, more clear and reliable information of the exfoliation and intercalation levels inside these composite samples were observed.

TEM Analysis

TEM images of the MMT platelet structures and dispersion patterns for the pure PAM and its nanocomposites with 1.0 and 2.0 wt % I-MMT are presented in Figure 1.

In the TEM pictures, the pure PAM morphology was white and transparent as the electron beam penetrated the sample, and a slight black part appeared at high magnification [Figure 1(a)]. This was due to the difference in the degree of electron-beam penetration for different parts of the sample. As shown in Figure 1(b,c), in the TEM micrographs of the nanocomposites with 1.0 and 2.0 wt % I-MMT, the dark lines represent the intersections of the MMT sheets, which were the cross sections of the MMT layers (marked with arrows). The original MMT layers were parallel, whereas the exfoliated layers were random. Meanwhile, some intercalated structures may have appeared inside the polymer matrix with increasing I-MMT loads. So, both exfoliated MMT platelets and intercalated stacks were visible [Figure 1(b,c)]. Because the MMT layers were composed of the heavier elements Al and Si and the interlayer was surrounded with by C, H, and O in the polymer matrix, darker lines appeared in the TEM micrographs.[27] These results show that the obtained HPAMNC mainly had exfoliated structures. This was consistent with XRD results (Figure 6).

Effect of I-MMT

The effects of the I-MMT load on the M_η, salt tolerance, temperature tolerance, and shear tolerance of the obtained samples were studied to obtain optimal reaction conditions for the production of the HPAMNC samples. The mass ratios of the reactive compositions are shown in Table I.

As shown in Table I, the initiation time and polymerization time decreased as the I-MMT load increased. However, the peak temperature increased from 84 to 88°C as the I-MMT load increased from 0.0 to 2.0 wt %. Because the high-activity exfoliated MMT platelets could absorb and disperse the initiator well into the polymer matrix, the polymerization reaction characteristics were significantly improved.[16] M_η increased from 5.83×10^6 to 8.51×10^6 when the I-MMT load increased from 0.0 to 1.0 wt % and then decreased from 8.51×10^6 to 4.51×10^6 when the I-MMT load increased from 1.0 to 2.0 wt %. This was because the highly active I-MMT absorbed —NH_2, —OH, and other polar groups in the PAM molecular chains. The PAM molecular chain aggregated in the I-MMT layers and formed partially crosslinked systems; this improved the polymer molecular dimension and the hydrodynamic volume. This made the system viscosity increase; this was similar to the reported literature.[21,22,34] An HPAMNC weak gel fabricated with a high viscosity was confirmed in the reported literature[21,22] and might have potential use in oil recovery.

Salt Tolerance. The salt tolerance of the samples was characterized by the retention value of the sample viscosity in a salt solution.[35,36] The viscosity variations of the samples in the NaCl and $CaCl_2$ solutions are shown in Figures 7 and 8.

As shown in Figures 7 and 8, the apparent viscosity of the pure PAM solution decreased from 22.12 to 12.51 mPa s as the concentration of the NaCl solution increased from 0.0 to 5000 mg/L. The apparent viscosity of HPAMNC with a 1.0 wt % I-MMT solution decreased from 27.43 to 18.15 mPa s as the concentration of the NaCl solution increased from 0.0 to 5000.0 mg/L. The apparent viscosity of HPAMNC with a 2.0 wt % I-MMT solution decreased from 21.65 to 14.52 mPa s as the concentration of the NaCl solution increased from 0.0 to 5000.0 mg/L. This phenomenon was similarly observed in $CaCl_2$ solutions with different concentrations. The salinity of the solution caused polymer molecular chain coils and resulted in decreases in their

Table I. Polymerization Parameters and Properties of the HPAMNC Samples

I-MMT load (%)	Initiation time (min)	Peak temperature (°C)	Polymerization time (min)	$M_\eta \times 10^6$
0.0	10.0	84.0	90.0	5.83
0.5	8.0	80.0	80.0	6.04
1.0	7.0	82.0	75.0	8.51
1.5	5.0	84.0	55.0	6.79
2.0	5.0	88.0	55.0	4.51

The initiation time is the time before polymerization starts; the peak temperature is the maximum exothermal temperature of polymerization.

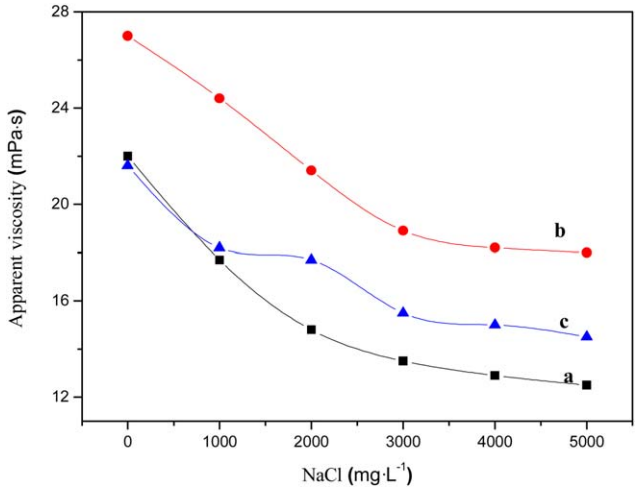

Figure 7. Curve of the apparent viscosity versus the NaCl solution concentration for samples of (a) pure PAM, (b) HPAMNC with 1.0 wt % I-MMT, and (c) HPAMNC with 2.0 wt % I-MMT. [Color figure can be viewed in the online issue, which is available at wileyonlinelibrary.com.]

molecular volumes and viscosities. This is typical behavior of polyelectrolytes.[37] The viscosities of HPAMNC with I-MMT (1.0 and 2.0 wt %) were higher than those of the pure PAM in the same salt solution. The viscosity of HPAMNC (2.0 wt %) was lower than that of HPAMNC (1.0 wt % I-MMT) because of the decrease in the molecular weight (see Table I). However, the decreasing tendency of the viscosity of the HPAMNC with 2.0 wt % I-MMT was much slower than that of HPAMNC with 1.0 wt % I-MMT, and the retention rate of the viscosity of the HPAMNC with 2.0 wt % I-MMT was higher than that of the HPAMNC with 1.0 wt % I-MMT. This was because the addition of I-MMT into the polymer matrix formed a unique organic–inorganic network structure. In this structure, the MMT platelets acted as a supermultifunctional crosslinker and enabled HPAMNC to form effective planes.[38] In addition, the surface of the organic modified MMT introduced long-chain alkyl hydrophobic groups; this resulted in improved salt tolerance in the composites. As shown in Figures 7 and 8, the effect of $CaCl_2$ on the viscosity of the composites was bigger than that of NaCl in the solution. Because the polarity of Ca^{2+} was higher than that of Na^+, the coils ratios of the macromolecular chains in the Ca^{2+} solution were much higher compared with that in the Na^+ solution; this resulted in a larger decrease in the hydrodynamic volume. These results clearly indicate that the proper MMT load increased the salt tolerance of the HPAMNC samples.

Temperature Tolerance. The temperature tolerance was investigated on both PAM and HPAMNC samples. At 30°C, the apparent viscosities of the pure PAM and HPAMNC solutions (1.0 and 2.0 wt % I-MMT) were 38.34, 75.11, and 44.78 mPa s, respectively. The apparent viscosities of these sample solutions decreased as the temperature increased (see Figure 8). However, the apparent viscosity of the HPAMNC solution was higher than that of the pure PAM under the same conditions. At high temperature, the viscosity difference between HPAMNC with 1.0 wt % I-MMT solution and pure PAM became larger. At 90°C, the viscosities of the pure PAM solution and HPAMNC with 1.10 wt % I-MMT were 11.81 and 41.62 mPa s, respectively. This may have been due to the fact that the movements of the polymer matrix macromolecular chains were restricted when the polymer molecular chains entered the galleries of MMT. The interactions between the MMT platelets further lowered their mobilities and resulted in a better temperature tolerance of HPAMNC.

Shear Tolerance. Shear tolerance is an important property for gels applied in petroleum engineering. At shear rate of 0.0 rpm, the apparent viscosities of the pure PAM and the HPAMNC solutions (1.0 and 2.0 wt % I-MMT) were 24.53, 128.34, and 39.12 mPa s, respectively. As shown in Figure 5, the apparent viscosities of these sample solutions decreased as the shear rate increased. At a shear rate of 100.0 rpm, the apparent viscosities of the pure PAM and the HPAMNC solutions (1.0 and 2.0 wt % I-MMT) were 10.03, 17.56, and 11.72 mPa s, respectively. Compared to the apparent viscosity of the HPAMNC with 2.0 wt % I-MMT, the apparent viscosity of the HPAMNC with 1.0 wt % I-MMT was much higher under the same shear rate because of its higher M_η. The phenomenon was attributed to the reduction of the diffusion rate of both the monomer molecules and active polymer chains in the viscose system.[39,40] These results show that the retention rate of the viscosity of HPAMNC was low. So, the antishearing properties still need to be improved further.

Morphology and Surface Behavior

The morphology and surface behavior of the HPAMNCs with 1.0 and 2.0 wt % I-MMT and their weak gels are shown in Figure 9.

As shown in Figure 9(a,b), I-MMT was well dispersed in the polymer matrix, and the HPAMNCs with 1.0 and 2.0 wt % I-MMT particles were in a line spherical shape with a diameter of 10.3 nm. The HPAMNC weak gels spontaneously assembled a regular arborization or cross-wire form on a cover glass during

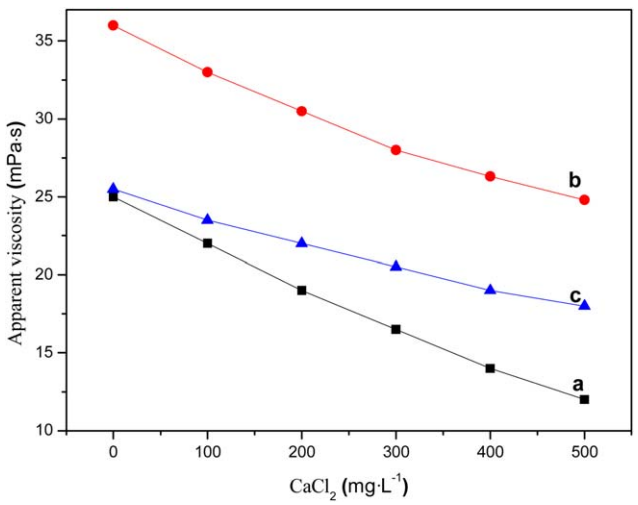

Figure 8. Curves of the apparent viscosity versus the $CaCl_2$ solution concentration for samples of (a) pure PAM, (b) HPAMNC with 1.0 wt % I-MMT, and (c) HPAMNC with 2.0 wt % I-MMT. [Color figure can be viewed in the online issue, which is available at wileyonlinelibrary.com.]

Table II. Synthesis Conditions of the PAMNC Weak Gels

No.	Sample	HPAMNC (mg/L)	Crosslinker (mg/L)	Thiourea (mg/L)	NaCl (mg/L)	pH	Dilution times
1	HPAMNC with 1.0 wt % I-MMT	4000	1000	200	5000	7.5	150
2	HPAMNC with 1.0 wt % I-MMT						200
3	HPAMNC with 2.0 wt % I-MMT						150
4	HPAMNC with 2.0 wt % I-MMT						200

The reactive temperature was 80°C; the reaction time was 2 h.

dried processing [Figure 9(c,d)]. This result has been reported little in the literature. The composition in the HPAMNC weak gels improved its temperature tolerance, salt tolerance, and shear tolerance and increased the elasticity and extensibility compared with the conventional gels; this was confirmed by Zolfaghari *et al.*[8] These properties made the nanocomposite weak gels more suitable as an in-depth profile modifier. So, the HPAMNC weak gels were better suited to high-temperature and high-salt-reservoir deep profile control requirements.

Particle Size and Size Distribution

The size and size distribution of the HPAMNC weak gels were tunable in the NaCl solution and were investigated with a dynamic laser light-scattering method. The synthesis conditions of the HPAMNC weak gels are presented in Table II. The obtained HPAMNC weak gel suspensions were diluted with deionized water to form a 4000 mg/L solution before measurement. The size and size distribution of the representative weak gel measured by dynamic laser light scattering are shown in Figure 10, and the measured data are summarized in Table III.

As shown in Figure 10, the size distribution of the HPAMNC in the 1.0 wt % I-MMT weak gels was polydispersed with a normal pattern in the water suspension. Such gel sizes and size distributions were easily tuned by variations in the suspension concentration, as shown in Table III. The *Z*-average value of the HPAMNC with 1.0 wt % I-MMT weak gel suspensions was approximately 494.0 nm when it was diluted 150 times with water. The *Z*-average value of HPAMNC with a 1.0 wt % I-MMT weak gel suspension was approximately 448.0 nm when it

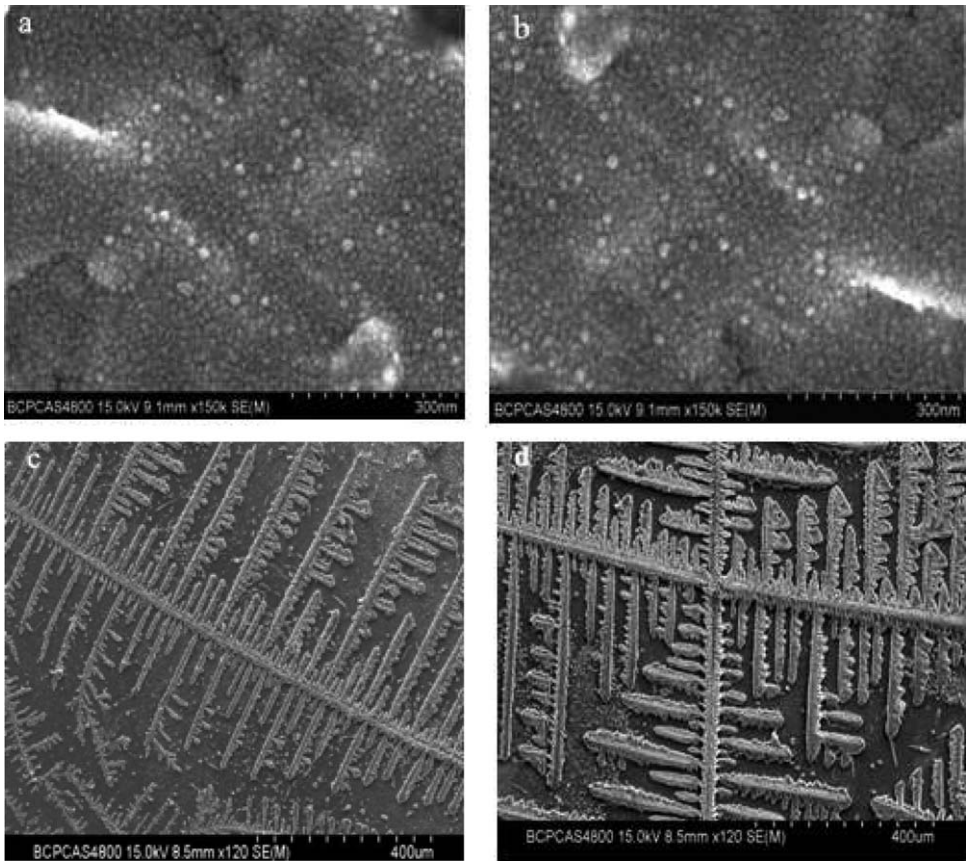

Figure 9. Morphology of (a) HPAMNC with 1.0 wt % I-MMT, (b) HPAMNC with 2.0 wt % I-MMT, (c) HPAMNC weak gel dried film with 1.0 wt % I-MMT, and (d) HPAMNC weak gel dried film with 2.0 wt % I-MMT.

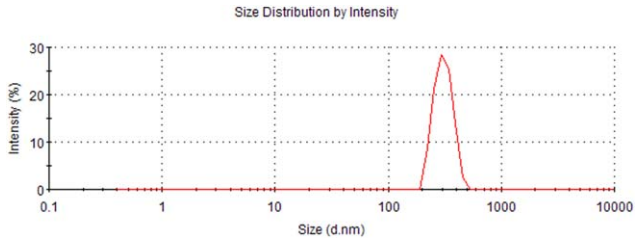

Figure 10. Dynamic laser scattering patterns of the size distribution of the representative HPAMNC weak gels in deionized water (HPAMNC with 1.0 wt % I-MMT, solution diluted by 150 times water). [Color figure can be viewed in the online issue, which is available at wileyonlinelibrary.com.]

was diluted 300 times with water. Similarly, the *Z*-average value of HPAMNC with a 2.0 wt % I-MMT weak gel suspension decreased from 422.0 to 404.0 nm as it was diluted with deionized water from 150 to 300 times. So, the mean diameters of the obtained nanocomposite weak gel suspensions were 300–500 nm; these values were reasonably larger than their practical diameters. We concluded that the gel association and distribution morphology could be tuned by variations in the gel suspension concentration of HPAMNC samples.

Thermal Properties

The static thermal stability of the pure PAM sample and HPAMNC (1.0 wt % I-MMT) was presented. The HPAMNC thermal stability was specially investigated under modeling environmental conditions. In this test, each sample was weighed within 0.5–1.0 g and put into the incubators, left for 30 min, and then put into a dryer for heating equilibrium. After they were cooled down, the samples' weight variations were carefully recorded. The weights against time curves were plotted for the HPAMNC sample weight against time under set temperatures of 90, 120, and 150°C, respectively. The thermal stability curves are shown in Figure 11(a–c).

As shown in Figure 11(a–c), both the pure PAM and HPAMNC sample weights decreased with increasing time. The weight loss of the HPAMNC samples was significantly smaller than that of pure PAM. This indicated that I-MMT effectively improved the thermal stability of the HPAMNC composite. In HPAMNC, the PAM polymer chains were adsorbed onto the MMT inorganic layer surface, which had a naturally high thermal tolerance and acted as a thermal shield. Moreover, their chain conformational entropy on the layer surface was significantly reduced, so it produced a high thermal stability.

Gel Solution Flooding Behavior in a Porous Channel

The sand pack tubes were processed by homogenization before the flooding experiments. The typical procedure was as follows: these multisized HPAMNC weak gel suspensions were used to flood in the porous channels of the sand pack tube models; the viscoelastic performance of the HPAMNC samples with optimized M_η and suspension concentration was achieved, and their gels were used to penetrate through different sizes of sand pack tube models to transfer the heterogeneous permeability to homogeneous permeability of the original channels. This was called a *homogenizing process*.

Gel-Flooding Behavior. The gel fluid flooding performance was determined in a flooding device where sand cores of both high and low permeability were fixed in hypertonic and hypotonic tubes, respectively.[39] In the water-flooding experiments, the oil recovery versus weak gel-flooding time curve was plotted on the basis of the two parallel unconsolidated sand tubes, in which one tube had a high permeability (1.80 μm^2) and the other tube had a low permeability (0.42 μm^2). The curve of the injection water versus flooding time is shown in Figures 12 and 13.

As shown in Figures 12 and 13, the oil-recovery rate increased quickly at the initial stage of water injection, and then, the oil elution volume reduced, and the water elution volume increased. After the initial water injection stage, the oil recovery increased slowly, and the water content decreased to the minimum level once the HPAMNC gel suspensions were flooded through the cores (Figure 13). These results strongly indicate that the HPAMNC coils or weak gels were effectively plugged in the fluid channels; this corresponded with the fact that the amount of water flowing through the same channel was significantly reduced. As the water volume accounted for 95% of the collected liquid, the oil-recovery rates in the hypertonic and hypotonic tubes were determined to be 64 and 34.8%, respectively.

Oil Recovery. After the water-flooding stage, once the HPAMNC weak gel suspension was injected into the previous porous core channels, the water content in the collected fluids was reduced. Then, as water was injected again after this weak gel suspension, the oil recovery was found to increase again markedly. In such process, the water content decreased rapidly at the beginning and then gradually increased. When the water volume in the collected fluids reached 95% again, the calculated oil-recovery rates in the hypertonic and hypotonic tubes were 99.1 and 81.0%, respectively. Thus, total net oil recovery increased relatively by 35.1 and 46.2%, respectively, as the cross-wire aggregated gels were used as

Table III. Weak Gel Sizes and Size Distributions by Dynamic Light Scattering

	Peak			
Sample	Gel diameter (nm)	Intensity (%)	Gel size distribution width (nm)	*Z*-average (nm)
HPAMNC with 1.0 wt % I-MMT	310.1	100.0	57.0	494.5
HPAMNC with 1.0 wt % I-MMT	473.3	78.2	159.5	447.9
HPAMNC with 2.0 wt % I-MMT	309.9	100.0	64.0	421.7
HPAMNC with 2.0 wt % I-MMT	384.1	84.2	123.8	404.9

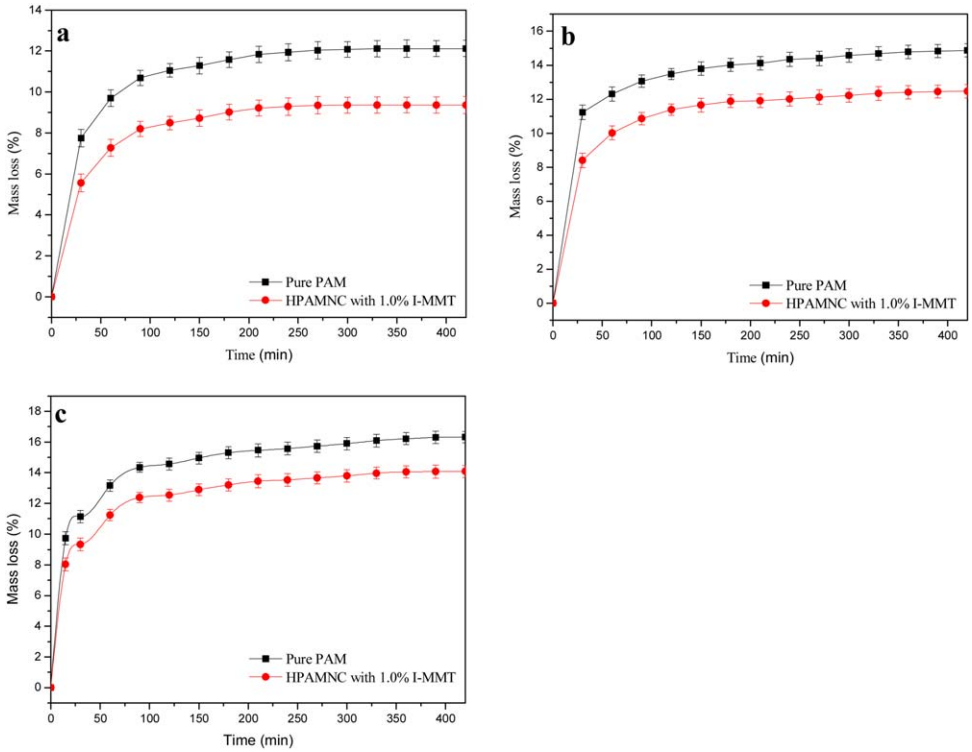

Figure 11. Thermal gravity curves versus aging temperatures for the pure PAM and PAMNC samples: (a) 90, (b) 120, and (c) 150°C. [Color figure can be viewed in the online issue, which is available at wileyonlinelibrary.com.]

the flooding fluids. These obtained net oil-recovery data were called the *enhanced oil-recovery rates*.

According to the results in the laboratory test, these nanocomposites may provide potential materials for modifying oil formation channels in practical oil recovery. Such a mechanism for modifying the channel surface and the flooding behaviors will be further investigated.

Gel Solution Fluidity. As the HPAMNC gel suspension concentration was well tuned, it had a high viscoelastic performance in the core pores. Stretching the HPAMNC gels in the suspensions easily produced a fiberlike and expandable morphology. This gel viscoelastic performance was required to form fiber flows in the porous core channels. The water absorption experiments of the dried

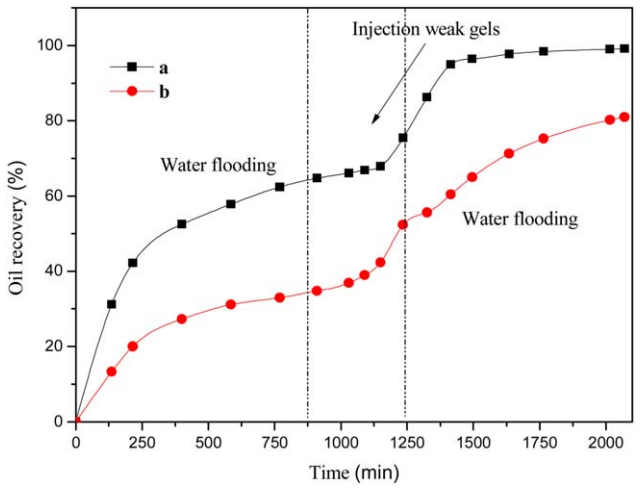

Figure 12. Curves of oil recovery versus the flooding time in sand pack tubes: (a) high-permeability sand pack tube and (b) low-permeability sand pack tube. The flooding quantity was 0.3 porous volumes of a weak gel solution, and the injection speed was 1.0 mL/min. The weak gels assembled at 70°C for some time. A saline solution was then injected at a flow rate of 1.0 mL/min. [Color figure can be viewed in the online issue, which is available at wileyonlinelibrary.com.]

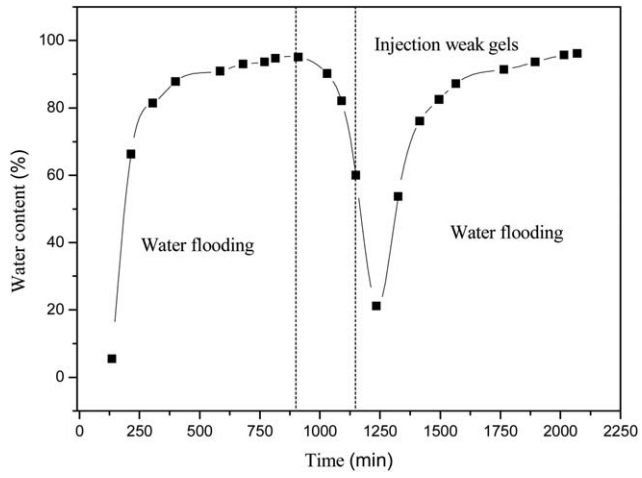

Figure 13. Curves of the water content of the recovered fluid versus the flooding time in sand pack tubes. The flooding quantity was 0.3 porous volumes of a weak gel solution, and the injection speed was 1.0 mL/min. The weak gels were then assembled at 70°C for some time. A saline solution was then injected at a flow rate of 1.0 mL/min.

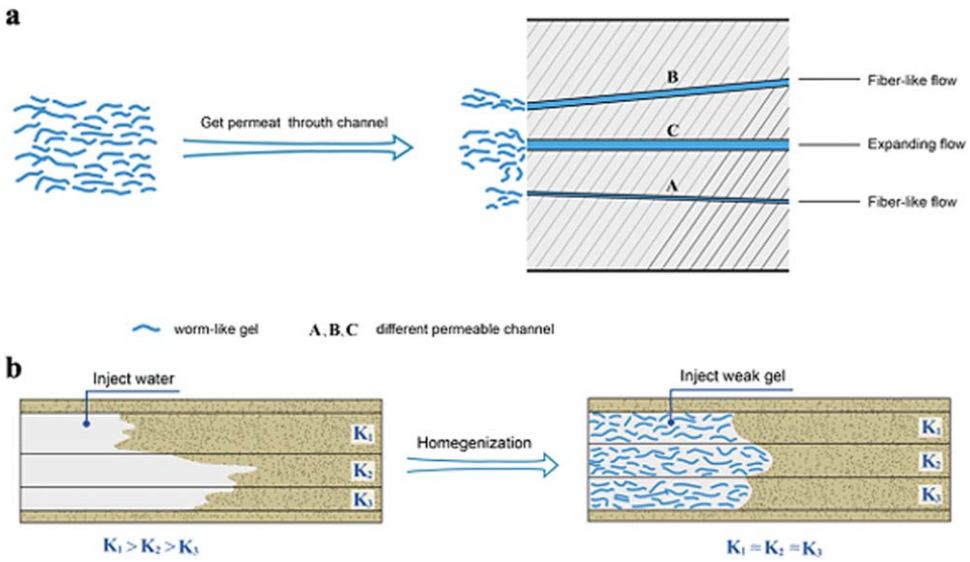

Figure 14. Proposed mechanism for the HPAMNC gel flooding and (a) enhancing flooding efficiency process and (b) homogenizing permeability process in the porous cores. [Color figure can be viewed in the online issue, which is available at wileyonlinelibrary.com.]

HPAMNC powders showed that they produced more than 60 times the expansion volume after they were in contact with water for a period of time. We concluded that, fiberlike and expandable flooding HPAMNC fluids permeated through the porous core channels to enhance their resistance to oil fluid flow, to homogenize pore channels, and finally to enhance the oil recovery.

Proposed Mechanism of the Gel-Flooding Behavior

The HPAMNC samples retained a similar viscoelastic and relaxation behavior as that of pure PAM.[41] Because of the molecular chain relaxation, some larger size HPAMNC gels had to deform in smaller pore channels and formed fiberlike fluids at shearing force. They exerted a high resistance to water fluid penetration in deeply fine channels via the hydration and self-assembling process.[42] Likewise, some of the HPAMNC gels were expanded in the lager pore channels to produce greater resistance coefficients and sweep volume inside the core channels. Thus, HPAMNC gels were able to enter both the hypertonic and hypotonic tubes (see Figure 2) driven by injected water. Their fiberlike and expandable flow patterns improved the sweep efficiency in core channels.

The mechanism for these gel-flooding effects was proposed and is shown in Figure 14(a). In the cores of three permeable channels, the permeability rate sequence was set as $C > B > A$. The cross-wire aggregated gels preferentially entered the most permeable channels with the largest pore diameter (C channel), then the B channel with the second larger pore diameter, and at last, the A channel with the smallest pore diameter in the unconsolidated sand cores.

The assembled cross-wire gels had a relatively high viscoelasticity and flow resistance to these fluids in the core channels; this forced the injected water flow to redirect. As the viscoelastic HPAMNC gels crawled through the core channels, its permeability was effectively homogenized. That is, as shown in Figure 14(b), the original permeability difference of K_1, K_2, and K_3 became $K_1 \approx K_2 \approx K_3$. This permeability homogenization process under a weak gel-flooding process effectively improved the oil recovery in the whole cores of heterogeneous permeability.

CONCLUSIONS

A novel I-MMT with a tunable layer structure was created, and its interlayer distance was tuned to about 1.42 nm with organic intercalants. Such intermediate was exfoliated into active layers and homogeneously dispersed *in situ* in a PAM matrix to improve M_η of the HPAMNC. The salt tolerance, temperature tolerance, and shear tolerances of the HPAMNC samples were higher than those of pure PAM. The cross-wire HPAMNC weak gel suspensions had good viscoelastic behaviors. They produced a tunable effect on the fluid flow redirection and a measurable enhanced oil-recovery rate of 46.2% compared to the original water-flooding process and could homogenize the permeability profile of oil formation. All of these results indicate that the HPAMNC weak gels could be a promising solution for enhanced oil recovery in the complex condition of petroleum engineering.

ACKNOWLEDGMENTS

The financial support of the Forward-Looking Guidance Project of China University of Petroleum (contract grant sponsor QZDX-2010-04), the National Major Project (contract grant sponsor 2011ZX05009-005), the Natural Science Foundation of China (contract grant sponsor 21076229), the Foundation for Innovative Research Groups of the National Natural Science Foundation of China (contract grant sponsor 51221003), and the Science Foundation of China University of Petroleum (contract grant sponsor KYJJ2012-06-30) is greatly appreciated.

REFERENCES

1. Okay, O.; Oppermann, W. *Macromolecules* **2007**, *40*, 3378.
2. Parmar, A. S.; Hill, S.; Vidyasagar, A.; Bello, C. B.; Toomey, R.; Muschol, M. *J. Appl. Polym. Sci.* **2013**, *127*, 1527.

3. Hurler, J.; Engesland, A.; Kermany, B. P.; Škalko-Basnet, N. *J. Appl. Polym. Sci.* **2011**, *125*, 180.
4. Singh, V. K.; Pal, K.; Pradhan, D. K.; Pramanik, K. *J. Appl. Polym. Sci.* **2013**, *130*, 1503.
5. Mitra, S.; Chattopadhyay, S.; Bhowmick, A. K. *J. Appl. Polym. Sci.* **2010**, *118*, 81.
6. Liu, Y.; Zhu, M.; Liu, X.; Zhang, W.; Sun, B.; Chen, Y.; Adler, H.-J. P. *Polymer* **2006**, *47*, 1.
7. Yeh, J. M.; Liou, S. J.; Chang, Y. W. *J. Appl. Polym. Sci.* **2004**, *91*, 3489.
8. Zolfaghari, R. A.; Katbab, A.; Nabavizadeh, J.; Tabasi, R. Y.; Nejad, M. H. *J. Appl. Polym. Sci.* **2006**, *100*, 2096.
9. Shibayama, M.; Suda, J.; Karino, T.; Okabe, S.; Takehisa, T.; Haraguchi, K. *Macromolecules* **2004**, *37*, 9606.
10. Haraguchi, K.; Li, H.-J.; Matsuda, K.; Takehisa, T.; Elliot, E. *Macromolecules* **2005**, *38*, 3482.
11. Tang, Q.; Lin, J.; Wu, Z.; Huang, M.; Yang, Y. *Eur. Polym. J.* **2007**, *43*, 2214.
12. Xu, J. S.; Ke, Y. C.; Zhou, Q.; Hu, X. L.; Tan, Z. J.; Yang, L. Y.; Song, Y. Z.; Zhao, Y. Y.; Zhang, G. L. *Polym. Compos.* **2014**, *35*, 1104.
13. Fischer, H. *Mater. Sci. Eng. C* **2003**, *23*, 763.
14. Liu, R.; Oppermann, W. *Macromolecules* **2006**, *39*, 4159.
15. Miyzaaki, S.; Karino, T.; Endo, H.; Kazutoshi, H.; Shibayama, M. *Macromolecules* **2006**, *39*, 8112.
16. Haraguchi, K.; Li, H. *J. Macromolecules* **2006**, *39*, 1898.
17. Hu, Z.; Ba, Z.; Xiong, W.; Gao, S.; Lu, R. *J. Daqing Pet. Inst.* **2006**, *3*, 51.
18. Xiong, C. M.; Tang, X. F. *Pet. Explor. Dev.* **2007**, *34*, 83.
19. Chen, K. S. Reservoir water control treatments using a non-polymer gelling system. Offshore South East Asia Show; Singapore, SPE, **1988**; p 17674.
20. Chang, H. L.; Sui, X. G.; Xiao, L.; Guo, Z. D.; Yao, Y. M.; Xiao, Y. G.; Chen, G.; Song, K. P.; James, C. M. *SPE Reservoir Eval. Eng.* **2006**, *9*, 664.
21. Xin, H. P.; Chen, H.; Wang, X. J.; Zhang, J.; Tan, Y. T. *J. Polym. Res.* **2013**, *20*, 311.
22. Shibayama, M.; Karino, T.; Miyazaki, S.; Okabe, S.; Takehisa, T.; Haraguchi, K. *Macromolecules* **2005**, *38*, 10772.
23. Huang, J. H.; Yang, L.; Wang, X. M.; Li, H. B.; Chen, L. M.; Liu, Y. N. *Chem. Eng. J.* **2014**, *248*, 216.
24. Chassenieux, C.; Nicolai, T.; Benyahia, L. *Curr. Opin. Colloid Interface Sci.* **2011**, *16*, 18.
25. Zhang, H.; Bai, B. *J. SPE J.* **2011**, *16*, 388.
26. Nikolaidis, A. K.; Achilias, D. S.; Karayannidis, G. P. *Eur. Polym. J.* **2012**, *48*, 240.
27. Xu, J. S.; Ke, Y. C.; Zhou, Q.; Hu, X. L. *J. Polym. Res.* **2013**, *20*, 195.
28. Liu, J. X.; Lu, X. G.; Liu, J. F.; Hu, S. Q.; Xue, B. Q. *Pet. Explor. Dev.* **2013**, *40*, 507.
29. Xin, H. P.; Chen, H.; Wang, X. J.; Zhang, J.; Tan, Y. B. *J. Polym. Res.* **2013**, *20*, 311.
30. Rabiee, A.; Zeynali, M. E.; Baharvand, H. *Iran. Polym. J.* **2005**, *14*, 603.
31. Jamal, A.; Ali, R. *J. Macromol. Sci. Phys.* **2008**, *47*, 98.
32. Fei, X.; Xu, S.; Feng, S.; Lin, J. L.; Lin, J. T.; Shi, X. M.; Wang, J. D. *J. Polym. Res.* **2011**, *18*, 1131.
33. Li, Y. M. High Polymer Physics Experiment, 3rd ed.; Zhejiang University Press: Hangzhou, China, **1996**; p 87.
34. Ma, J. T.; Liang, B.; Cui, P.; Dai, H.; Huang, R. H. *Polymer* **2003**, *44*, 1281.
35. Feng, Y. J.; Billon, L.; Grassl, B.; Bastiat, G.; Borisov, O.; Francois, J. *Polymer* **2005**, *46*, 9283.
36. Guo, Y. J.; Liu, J. X.; Zhang, X. M.; Feng, R. S.; Li, H. B.; Zhang, J.; Lv, X.; Luo, P. Y. *Energy Fuels* **2012**, *26*, 2116.
37. Wu, Y. M.; Zhang, B. Q.; Wu, T.; Zhang, C. G. *Colloid Polym. Sci.* **2007**, *279*, 836.
38. Miyazaki, S.; Karino, T.; Endo, H.; Haraguchi, K.; Shibayama, M. *Macromolecules* **2006**, *39*, 8112.
39. Puntervold, T.; Strand, S.; Austad, T. *Energy Fuels* **2007**, *21*, 1606.
40. Polacco, G.; Oakka, N.; Senubi, D. *Polym. Int.* **1999**, *483*, 92.
41. Xiong, L. J.; Hu, X. B.; Liu, X. X.; Tong, Z. *Polymer* **2008**, *49*, 5064.
42. Petit, L.; Karakasyan, C.; Pantoustier, N. *Polymer* **2007**, *48*, 7098.